Wadkins, R. M., & Jovin, T. M. (1991) *Biochemistry 30*, 9469-9478.
Wang, A. H.-J., Fujii, S., van Boom, J., & Rich, A. (1982) *Proc. Natl. Acad. Sci. U.S.A. 79*, 3968-3972.
Waring, M. J. (1970) *J. Mol. Biol. 54*, 247-279.
Wells, R. D., & Larson, J. E. (1970) *J. Mol. Biol. 49*, 319-342.
Wilson, W. D., Jones, R. L., Zon, G., Scott, E. V., Banville, D. L., & Marzille, L. G. (1986) *J. Am. Chem. Soc. 108*, 7113-7114.

Probing Structural Factors Stabilizing Antisense Oligonucleotide Duplexes: NMR Studies of a DNA·DNA Duplex Containing a Formacetal Linkage

Xiaolian Gao,* Frank K. Brown, and Peter Jeffs

Structural and Biophysical Chemistry, Glaxo Inc. Research Institute, Five Moore Drive, Research Triangle Park, North Carolina 27709

Norbert Bischofberger and Kuei-Ying Lin

Gilead Sciences, Inc., 346 Lakeside Drive, Foster City, California 94404

Adrian J. Pipe and Stewart A. Noble

Department of Medicinal Chemistry, Glaxo Group Research Limited, Greenford Road, Greenford UB6 OHE, United Kingdom

Received November 27, 1991; Revised Manuscript Received April 21, 1992

ABSTRACT: The duplex formed by annealing the formacetal backbone modified dodecamer d-(CGCGTT$_{OCH_2O}$TTGCGC) to its complementary strand, d(GCGCAAAACGCG) (duplex I), has been studied by NMR techniques and analyzed with reference to its unmodified counterpart (duplex II). Comparison of parameters such as 2D cross-peak intensities, coupling constants, and spectral patterns indicates that structural perturbations caused by the incorporation of the formacetal linkage are minimal and localized to the central T_4·A_4 block. Duplex I adopts a B-type helical conformation with regular Watson–Crick base pairing and normal minor groove width. The methylene group is accommodated along the phosphate backbone in a conformation similar to that of the PO_2 group found in the B-form DNA family. The central T6-T7 base pairs of duplex I melt simultaneously with the duplex, indicating a cooperative transition to single strands. Although the formacetal linkage affects global melting, as evidenced by a 3 °C reduction in T_m for duplex I with respect to duplex II, the present study indicates that this is not the result of localized premelting at the formacetal site of duplex I but rather reflects the subtle interplay of several structural and energy factors which need to be further explored.

The idea of preventing gene transcription and/or gene translation at the DNA/mRNA level is an attractive one for many reasons. Classical approaches to drug discovery involve the design and identification of compounds directed against enzymes, receptors, or ion channels, the structure and mode of action of which are usually complex and often poorly understood. Conversely, the potential for therapeutic intervention at the nucleic acid level follows a well-ordered, generalizable strategy which is targeted at the initiating events of an amplifying cascade: transcription of a gene gives rise to many copies of mRNA which on translation affords an even greater number of protein molecules. Inhibition of gene expression ought, therefore, to be more efficient than inhibition of the gene product.

The potential of oligonucleotides (ODNs) to serve as code-blocking therapeutic principles was first recognized by Stephenson and Zamecnik (1978). Stimulated by their findings, interest in ODNs as sequence-specific code blockers has grown steadily over recent years [reviewed by Uhlmann and Peyman (1990) and Miller (1991)]. Whether the intended use is as an antisense or triplex agent, the requirement is for ODNs which are stable to both extracellular and intracellular enzymes and capable of being transported to their site of action. In chemical terms this means that some or all of the usual phosphodiester linkages must be replaced with nuclease-stable and preferably nonpolar surrogates which still allow for hybridization. Not surprisingly, initial attention focused on close phosphodiester analogues and attempted to preserve the central role of phosphorus. Methylphosphonates, alkyl phosphotriesters, phosphorothioates, and phosphoramidates typify the first-generation analogues [reviewed by Uhlmann and Peyman (1990)]. Although such modifications impart ODN stabilization and are claimed by some to show promise in enhancing cellular permeability, they often result in reduced binding affinity as judged by T_m depression when compared with phosphodiester counterparts and introduce an additional complication in that substitution of one phosphate oxygen atom in a phosphodiester linkage generates a new center of chirality (Pramanik & Kan, 1987; Froehler & Matteucci, 1988; Lin et al., 1989; Kibler-Herzog et al., 1991; Dagle et al., 1991; Piotto et al., 1991; Kibler et al., 1991). This latter issue is problematical, since biological systems are known to discriminate between enantiomers, and becomes acute in the context of a multiply modified oligomer where each stereoisomer is likely to possess a unique biological profile. An elegant solution to this problem is to only target achiral

0006-2960/92/0431-6228$03.00/0

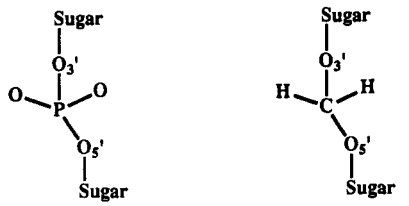

Phosphate diester Formacetal linkage

FIGURE 1: Phosphate diester linkage in native nucleic acids and its formacetal surrogate.

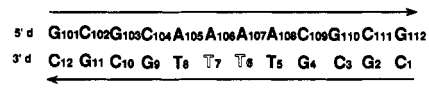

FIGURE 2: The sequence being studied where the formacetal linkage is incorporated into the T6–T7 step (duplex II). Duplex I is the natural phosphodiester dodecamer.

phosphodiester surrogates, and examples of a second generation of non-phosphate linkages are now emerging (Matteucci, 1990; Veeneman et al., 1991; Nielson et al., 1988; Schneider & Benner, 1990, 1991).

Although there has been rapid accumulation of information concerning the chemical synthesis of backbone-modified ODNs and their biophysical and biochemical properties, our understanding of the implications of such modification on complex formation as revealed by study of three-dimensional structure is in its infancy. Thus far, only three duplexes containing modified backbone moieties have been probed by crystallographic means. Of particular note is the work of Cruse et al. (1986), who reported the crystal structure of the self-complementary duplex (R_p)-d[G(S)CG(S)CG(S)C] [*R* chirality; (S) represents phosphorothioate], and that of Heinemann et al. (1991), who studied the effect of a single 3'-methylene phosphonate linkage on the conformation of d-(GCCCG*p*GGC). In addition, a report on the complex formed between 11-deoxydaunomycin and the (R_p)-d[CGT(S)ACG] duplex (S: phosphorothioate in an *R* configuration) has appeared (William et al., 1990). In each case the modification was shown to be readily accommodated within the known structural framework of duplex DNA. Clearly an understanding of solution structure is vital for the development of genetic targeting as a novel therapeutic strategy. As yet, little information pertaining to the detailed solution structure elucidation of complexes containing phosphate backbone modified ODNs has appeared in the literature. This initial report concerns the determination of the solution structure of a DNA duplex in which one strand contains a single modified linkage by NMR techniques. Our particular interest is the formacetal linkage (Figure 1) which has recently been introduced as an achiral, neutral, phosphodiester isostere (Matteucci, 1990; Veeneman et al., 1991). Formacetal-linked ODNs show considerable promise as code-blocking agents since they bind to RNA and ss- and dsDNA, are stable to exonuclease attack, and manifest enhanced cellular uptake characteristics. The system chosen for study is depicted in Figure 2, which comprises two non-self-complementary dodecamers. Formacetal incorporation into the T6-T7 site affords duplex I, which was subjected to 2D ^{1}H NMR spectroscopic analysis. Comparison of NMR parameters derived from this study for duplex I with those obtained from its phosphodiester counterpart, duplex II, allowed detailed characterization of these structures and a parallel analysis of the structural perturbations attributable to the incorporation of the formacetal linkage. In addition, the present work provides an experimental basis on which to found predictive modeling of modified ODNs involving acetal-related linkages and represents a stepping off point for the study of RNA·DNA heteroduplexes in the class.

Materials and Methods

The phosphodiester oligonucleotides d-(GCGCAAAACGCG) and d(CGCGTTTTGCGC) were assembled by phosphoramidite chemistry (McBride & Caruthers, 1983) on 30 μM scale using an ABI 380B DNA synthesizer. A two-stage HPLC purification method was employed. Chromatography on PRP-1 [Hamilton; (A) 0.1 M TEAA, pH 7.0; (B) CH_3CN, 5–80% (B) in 50 min] was used to select for trityl-positive material. Following treatment with 80% aqueous acetic acid, final purification was by chromatography on a C_{18} column [Dynamax; 300 Å, 12 μm, 21 × 250 mm; (A) 0.1 M TEAA, pH 7.0; (B) CH_3CN, 0–30% (B) over 50 min]. The oligonucleotide d-(CGCGTT$_{OCH_2O}$TTGCGC) was assembled by the H-phosphonate chemistry (Froehler, 1986), employing pivaloyl chloride as the activating agent. The formacetal linkage was introduced by dimer block coupling of the T$_{OCH_2O}$T unit, which was prepared by a variation of a published procedure (Matteucci, 1990). Thus, to a mixture of 5'-*O*-DMT-3'-*O*-[(methylthio)methyl]-T (0.9 g, 1.5 mmol), 3'-*O*-TBDMS-T (0.8 g, 2.2 mmol), 2,6-diethylpyridine (1.0 g, 7.4 mmol), and molecular sieves (4 A, 2.0 g) in dry benzene (60 mL) stirred at room temperature for 1 h was added a solution of bromine in benzene (1.5 mL, 1.0 M, 1.5 mmol). The mixture was stirred at room temperature for a further 2 h and then washed with saturated aqueous sodium bicarbonate solution. The organic solution was separated, dried (Na_2SO_4), and evaporated to dryness. The residue was dissolved in dry THF (10 mL) and treated with a solution of TBAF in THF (4.0 mL, 1.0 M, 4 mmol). The mixture was stirred at room temperature for 30 min, concentrated, dried (Na_2SO_4), and evaporated to dryness. The residue was purified by flash column chromatography on silica gel employing a gradient of 1% TEA/CH_2Cl_2 to 1% TEA/5% MeOH/CH_2Cl_2 as the mobile phase. Fractions containing the desired material were pooled and evaporated to afford the 5'-*O*-DMT-protected T$_{OCH_2O}$T dimer block (0.84 g, 71% yield) as a colorless foam. Spectral data were consistent with the proposed structure. H-phosphonate derivatization was achieved by standard procedures (Froehler, 1986). Purification of the formacetal oligomer was achieved by RP-HPLC on C_{18} silica as previously described. In excess of 1000 OD (~10 mg) of each purified oligomer was obtained.

The synthetic oligonucleotide sequences were characterized by PAGE, CZE (capillary zone electrophoresis), HPLC (reverse phase and anion exchange), and mass spectral analysis. The formacetal-containing oligomer was retained slightly less than the corresponding phosphodiester-linked ODN on ion-exchange HPLC. Base compositional analysis of the formacetal oligomer following P1 nuclease and alkaline phosphatase digestion showed the presence of dG, dC, dT, and T$_{OCH_2O}$T in the predicted ratios. Mass spectra were recorded using a PE Sciex API-III mass spectrometer in the negative ion mode. Samples were dissolved in aqueous ammonium bicarbonate (5 mM)/acetonitrile (1:1 v/v, pH 8.5) and were infused into the instrument at 2 μL/min. The orifice voltage was −70 V. The mass range was scanned from m/z 300 to m/z 1600 at ca. 25 s/scan. Spectra were coadded (five to eight scans) to improve the signal to noise ratio. Molecular masses were assigned using the Hyermass software in the MS data system. All three oligomers gave the expected molecular ions.

Prior to optical T_m and NMR studies, the oligomers were converted to their sodium form by treatment with Dowex 50X8 Na^+ resin. Thermal melting studies were conducted on a

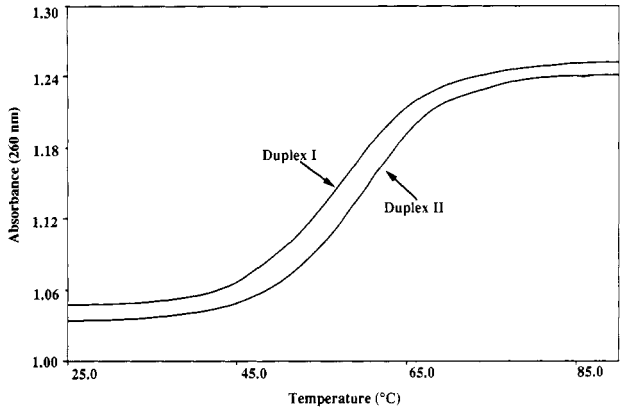

FIGURE 3: Temperature profile of UV (260 Å) absorption of duplex I and duplex II (see Materials and Methods for experimental conditions). Applying first derivative analysis results in T_ms of 57 and 60 °C for duplex I and duplex II, respectively.

Gilford Response II UV spectrophotometer equipped for thermoprogramming. T_m curves were obtained as follows: 0.3 OD of each of the complementary strands was combined, dried down, and dissolved in 10 mM NaH_2PO_4 and 150 mM NaCl, pH 7.4 (0.5 mL). The temperature was ramped from 25 to 90 °C at a rate of 0.5 °C per minute and A_{260} monitored. First derivative analysis of the absorbance curves yielded T_m data. The melting curves for duplex I and duplex II are shown in Figure 3, with T_ms of 57 and 60 °C, respectively.

NMR experiments were performed on a Bruker AMX500 spectrometer. ODN duplex annealing was monitored by 1D NMR experiments, and the final NMR samples contained 3–4 mM duplex in aqueous buffer (0.1 M NaCl, 10 mM phosphate, 0.1 mM EDTA, pH 6.2). Proton NOESY spectra of duplex I and duplex II were recorded at 15 °C (mixing times of 100 and 150 ms, H_2O) and 25 and 35 °C (mixing times of 100 and 250 ms, D_2O). In addition, DQF-COSY, TOCSY (mixing time 50 ms), and COSY-35 spectra of duplex I and duplex II were recorded at both 25 and 35 °C in D_2O. The NMR data matrix contains 2048 or 1024 complex data points in the t_2 dimension and 512–1024 real points in the t_1 dimension. Preacquisition delays were to 1.2–2.0 s. Data were processed and analyzed using the Felix program (Hare Research). Distances were derived from NOE connectivities on the basis of a two-spin approximation (Neuhaus & Williamson, 1989). Scalar coupling constants for sugar H1′,H2′ and H1′,H2″ protons were measured from COSY-35 spectra, which experimentally are similar to those of COSY-45 (Derome, 1987), and were obtained by utilizing a 35° detection pulse. The chemical shifts of ^{31}P resonances were measured by referencing to that of an external trimethyl phosphate sample in aqueous buffer solution (0.1 M NaCl). ^1H–^{31}P correlation spectra were recorded in the ^1H detection mode with a pulse described by Sklenar et al. (1986) with ^{31}P 90° pulse cycling in phase with the detector.

RESULTS

Exchangeable Protons

Chemical Shifts and NOE Cross Peaks. The expanded NOESY spectra correlating imino (F_2) with base (F_1) proton resonances for duplex I and duplex II in water are given in Figure 4. The chemical shifts of the imino and amino protons are listed in Table I. The imino protons of T5–T8 in both duplex I and duplex II exhibit well-resolved resonances which appear in a spectral region (13.5–14.0 ppm) characteristic of A·T Watson–Crick base pairing. A comparison of the chemical shifts for the imino protons of duplex I and duplex II is

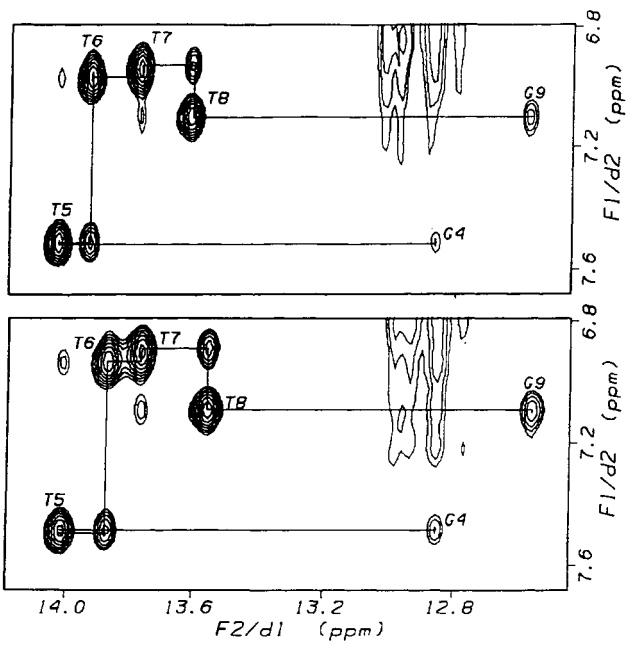

FIGURE 4: Expanded NOESY (150-ms mixing time) spectra recorded in H_2O at 15 °C: upper panel, unmodified duplex II; lower panel, formacetal-containing duplex I. The spectral region covers imino protons (F_2) and adenine H2 protons (F_1). Solid lines in both spectra mark sequential connectivities from A108(H2) to G4(HN), T5(HN), and T6(HN), from A107(H2) to T6(HN) and T7(HN), and from A106(H2) to T7(HN) and T8(HN), as well as from A105(H2) to T8(HN) and G9(HN).

depicted in Figure 5. The proton resonances of T6 and T8 in duplex I are slightly shifted upfield relative to their counterparts in duplex II. Sequential NOE connectivities linking thymine HN protons to adenine H2 protons within the context of a single base pair and to those of adjacent residues are shown in Figure 4. Thus, T8 (HN, 13.59 ppm), for example, exhibited two NOE cross peaks: the stronger one was assigned to its interaction with A105 (H2, 7.06 ppm) of the same base pair, the weaker one with A106 (H2, 6.90 ppm) of the adjacent base pair.

Temperature Dependence of Imino Proton Resonances. The transition of duplex I and duplex II to single strands was monitored by recording temperature-dependent spectra of the imino protons (Figure 6). The resonances of T5(HN) and T6(HN) in duplex I and duplex II were both shifted upfield at elevated temperatures, whereas those associated with T7(HN) and T8(HN) were unaffected. The imino resonances for G2 and G11 exhibited similar line broadening at 41 and 47 °C for duplex I and duplex II, respectively. The eight imino protons associated with the central T_4·A_4 block of both duplex I and duplex II melted in a cooperative manner at 57 and 60 °C, respectively.

Nonexchangeable Protons

Sequential NOE Connectivities. NOESY spectral regions for duplex I and duplex II in which base protons appear along the F_2 axis and sugar H1′ protons along the F_1 axis are shown in Figure 7. Sequential NOE connectivities linking protons of a given heterocyclic base to its own H1′ proton and to the H1′ proton of its adjacent 5′ residue were well-defined for both duplex I and duplex II (Figure 7). All of the base and sugar H1′, H2′, H2″, H3′, and H4′ resonances were assigned by a combination of base and sugar proton sequential NOE and coupling cross-peak analyses (Table I).

Cross-Strand NOE Cross-Peak Intensities. Adenine H2 protons reside in the minor groove of duplex DNA and are

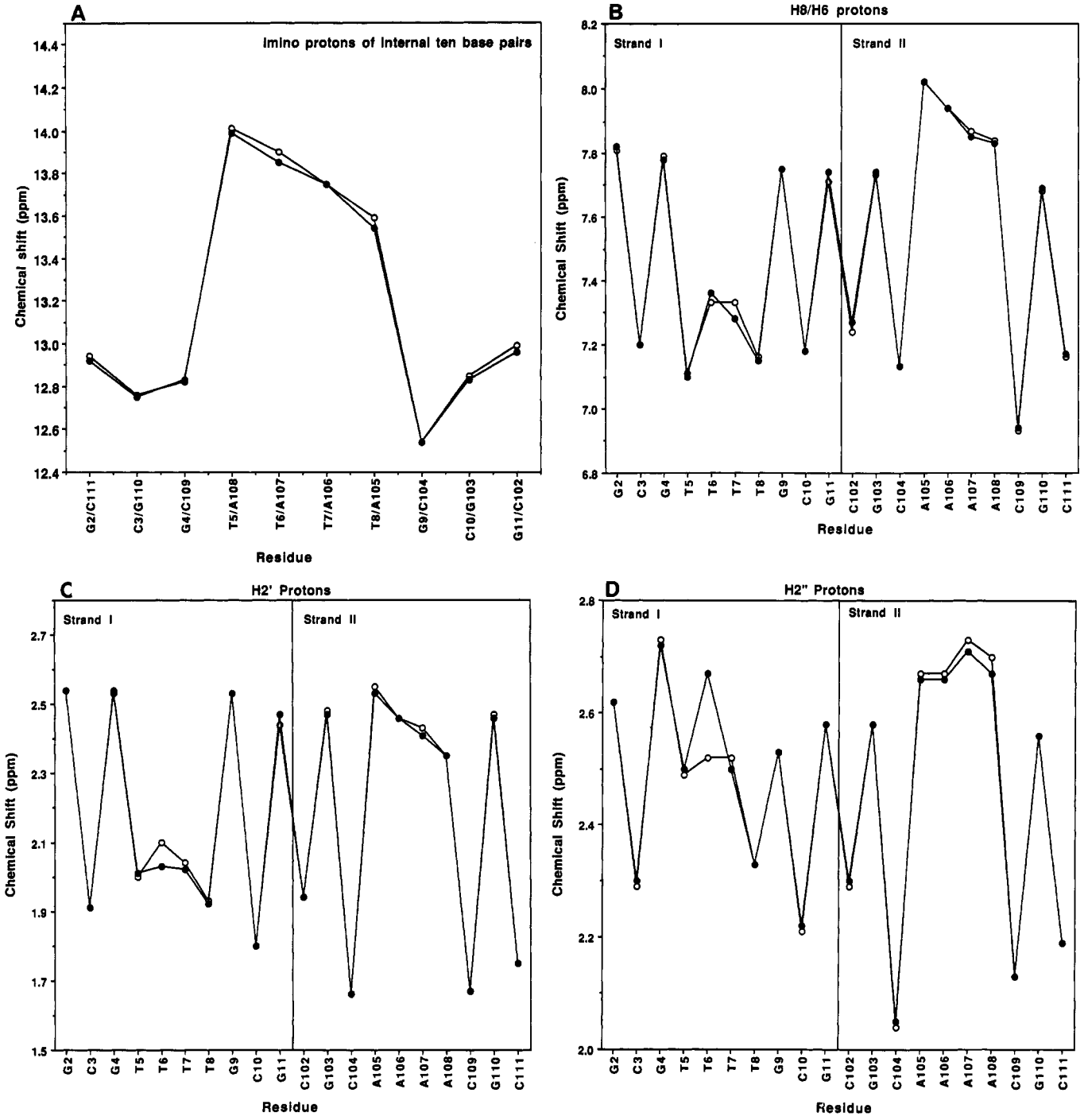

FIGURE 5: Chemical shift comparisons of duplex I (solid circle) and duplex II (open circle) under comparable experimental conditions. Chemical shifts of (A) imino protons of the duplexes, (B) base H8 and H6 protons, (C) H2′ protons, and (D) H2″ protons are shown.

less than 5 Å from the H1′ protons of both intraresidues and 3′-adjacent residues. Additionally, adenine H2 protons often exhibit NOEs to the H1′ protons of residues within its complementary strand (cross-strand NOE), as depicted in Figure 7. The adenine H2 resonances associated with the central T_4·A_4 block of duplex I and duplex II were detected as shown in panels A and C of Figure 7. The aforementioned NOE cross peaks were assigned and are listed with their corresponding integration volumes in Table II.

Chemical Shifts. The chemical shifts corresponding to the base, H2′, and H2″ of the peripheral four residues of duplex I and duplex II differ by less than 0.02 ppm (Figure 5B–D). Deviations in chemical shift were detected around the central T_4·A_4 block of duplex I as shown in Figure 5B–D and Table I. The largest upfield shifts (0.3 and 0.57 ppm) were observed for T6(H3′) and T7(H5′ or H5″) proton resonances of duplex I as compared to those of duplex II. The base and H1′ protons of the T6 residue of duplex I resonated at 0.02–0.03 ppm downfield, and the T7 residue resonated 0.02–0.05 ppm upfield of the corresponding protons in duplex II. Additionally, T6-(H2″) of duplex I exhibited a 0.07-ppm upfield shift, while T6(H2′) shifted 0.13 ppm downfield relative to duplex II.

COSY Cross-Peak and Coupling Constants. COSY-35 spectra of duplex I and duplex II produced simplified coupling cross peaks at the expense of reduced intensities of peaks close to the diagonal. Expanded COSY-35 spectral regions containing H1′ (F_2) and H2′,H2″ (F_1) resonances for duplex I and duplex II are shown in Figure 8. All COSY cross peaks in these spectra were assigned; for simplicity only those arising from the central six base pairs are identified in Figure 8. Each

Table I: Chemical Shifts of DNA·DNA Formacetal Duplex I and Unmodified DNA·DNA Duplex II[a]

	HN	NH_2	H8	H2	H6	H5	H1′	H2′	H2″	H3′	H4′	H5′,H5″
						DNA·DNA Duplex II						
C1					7.45	5.71	5.59	1.79	2.25	4.55	3.94	
G2	12.94	7.2–6.6	7.81				5.77	2.54	2.62	4.85	4.23	
C3		8.22/6.33			7.20	5.25	5.55	1.91	2.29	4.72	4.07	
G4	12.82	7.2–6.6	7.79				5.91	2.53	2.73	4.86	4.29	
T5	14.01				7.11	1.31	5.90	2.00	2.49	4.73	4.15	
T6	13.90				7.33	1.48	6.04	2.10	2.52	4.78	4.08	
T7	13.75				7.33	1.53	6.00	2.04	2.52	4.79	4.09	4.10 ± 0.10
T8	13.59				7.16	1.56	5.69	1.93	2.33	4.78	4.01	
G9	12.54	not seen	7.75				5.68	2.53	2.53	4.86	4.25	
C10		8.17/6.30			7.18	5.22	5.56	1.80	2.21	4.68	4.03	
G11	12.99	7.2–6.6	7.71				5.79	2.44	2.58	4.83	4.20	
C12		8.10/6.37			7.16	5.04	5.98	2.08	2.08	4.35	3.88	
G101			7.78				5.79	2.45	2.63	4.72	4.15	
C102		8.30/6.33			7.24	5.21	5.62	1.94	2.29	4.74	4.04	
G103	12.85	7.2–6.6	7.78				5.73	2.48	2.58	4.84	4.22	
C104		8.26/6.25			7.13	5.27	5.27	1.66	2.04	4.64	3.95	
A105		6.23/6.02	8.02	7.06			5.58	2.55	2.67	4.88	4.21	
A106		6.04/5.73	7.94	6.90			5.62	2.46	2.67	4.90	4.27	
A107		6.07/5.76	7.87	6.93			5.73	2.43	2.73	4.89	4.29	
A108		6.09/5.93	7.84	7.46			5.89	2.35	2.70	4.85	4.30	
C109		7.82/6.30			6.93	4.91	5.45	1.67	2.13	4.64	3.98	
G110	12.76	7.2–6.6	7.68				5.71	2.47	2.56	4.83	4.21	
C111		8.30/6.44			7.16	5.25	5.63	1.75	2.19	4.68	4.03	
G112			7.76				6.00	2.50	2.26	4.55	4.05	
						DNA·DNA Formacetal Duplex I						
C1					7.48	5.75	5.64	1.81	2.26	4.57	3.94	
G2	12.92	7.2–6.6	7.82				5.79	2.54	2.62	4.85	4.23	
C3		8.20/6.34			7.20	5.26	5.57	1.91	2.30	4.72	4.07	
G4	12.83	7.2–6.6	7.78				5.92	2.54	2.72	4.86	4.26	
T5	13.99				7.10	1.32	5.90	2.01	2.50	4.71	4.14	
T6	13.85				7.36	1.49	6.06	2.03	2.67	4.48	4.02	3.93/3.96
T7	13.75				7.28	1.51	5.97	2.02	2.50	4.75	4.09	3.53/4.22, 4.80/4.94[b]
T8	13.54				7.15	1.56	5.70	1.92	2.33	4.76	4.01	
G9	12.54	not seen	7.75				5.70	2.53	2.53	4.85	4.25	
C10		8.17/6.30			7.18	5.23	5.58	1.80	2.22	4.68	4.03	
G11	12.96	7.2–6.6	7.74				5.81	2.47	2.58	4.84	4.20	
C12					7.25	5.22	6.02	2.06	2.06	4.35	3.90	
G101			7.80				5.83	2.46	2.64	4.72	4.12	
C102		8.22/6.31			7.27	5.25	5.62	1.94	2.30	4.74	4.06	
G103	12.83	7.2–6.6	7.74				5.75	2.47	2.58	4.84	4.20	
C104		8.25/6.25			7.13	5.28	5.30	1.66	2.05	4.65	3.95	
A105		6.23/6.02	8.02	7.09			5.58	2.53	2.66	4.88	4.20	
A106		6.04/5.73		7.94	6.93		5.63	2.46	2.66	4.89	4.26	
A107		6.07/5.76	7.85	6.94			5.71	2.41	2.71	4.88	4.27	
A108		6.09/5.93	7.83	7.47			5.90	2.35	2.67	4.84	4.28	
C109		7.79/6.30			6.94	4.92	5.46	1.67	2.13	4.63	3.99	
G110	12.75	7.2–6.6	7.69				5.72	2.46	2.56	4.83	4.20	
C111		8.26/6.42			7.17	5.27	5.65	1.75	2.19	4.68	4.03	
G112			778				6.02	2.48	2.27	4.55	4.04	

[a] Data for exchangeable protons were from 150-ms mixing time NOESY recorded in 0.1 M NaCl, 10 mM phosphate, and 0.1 mM EDTA, 290 K, pH 6.2, with chemical shifts referenced to that of the HOD resonance (δ = 4.80 ppm). Data for nonexchangeable protons were from 250-ms mixing time NOESY recorded at 308 K with chemical shifts referenced to that of the HOD resonance (δ = 4.58 ppm). [b] Acetal methylene protons T7(HP1,HP2).

H1′ proton is coupled to H2′ and H2″; furthermore, coupling cross peaks of H3′ to H2′ were discernible in DQF-COSY spectra. The COSY-35 coupling cross-peak patterns for duplex I closely resemble those of duplex II. $J_{1'2'}$ and $J_{1'2''}$ coupling constants as well as the estimation of $J_{3'4'}$ obtained with those related to the central T_4·A_4 block for duplex I and duplex II are given in Table III.

NOEs Related to the Formacetal Methylene Protons. The methylene protons of the formacetal linkage of duplex I are T7(HP1) and T7(HP2) and resonate at 4.95 and 4.80 ppm, respectively. NOE cross peaks arising from interactions of these protons with T6(H1′), T6(H3′), and T7(H5′,H5″) are depicted in Figure 9; a more complete list of NOE cross-peak assignments is given in Table IV. Cross-peak intensities were converted to distances and are compared with those measured between phosphate oxygens and adjacent sugar protons within a 5-Å radius in a B-form DNA model in Table IV.

^{31}P NMR Spectra. ^{31}P 1D and ^{1}H–^{31}P 2D NMR spectra (^{1}H detection) demonstrate that phosphate ^{31}P of duplex I and duplex II resonates at 3.9–4.5 ppm upfield from that of an external trimethyl phosphate reference, resulting in a chemical shift dispersion of less than 0.6 ppm.

Discussion

The detailed solution structure analysis of DNA by ^{1}H NMR techniques is intrinsically constrained by the limited numbers of protons present in nucleotides. Our approach to probing the effect of analogue incorporation on recognition parameters and duplex structure in particular relies on detecting perturbations in the structure rather than its absolute determination. Thus, our attention has focused on the comparison of two related duplex structures, one containing a single formacetal linkage, d(CGCGTT$_{OCH_2O}$TTGCGC), and its complementary strand, d(GCGCAAAACGCG) (duplex I),

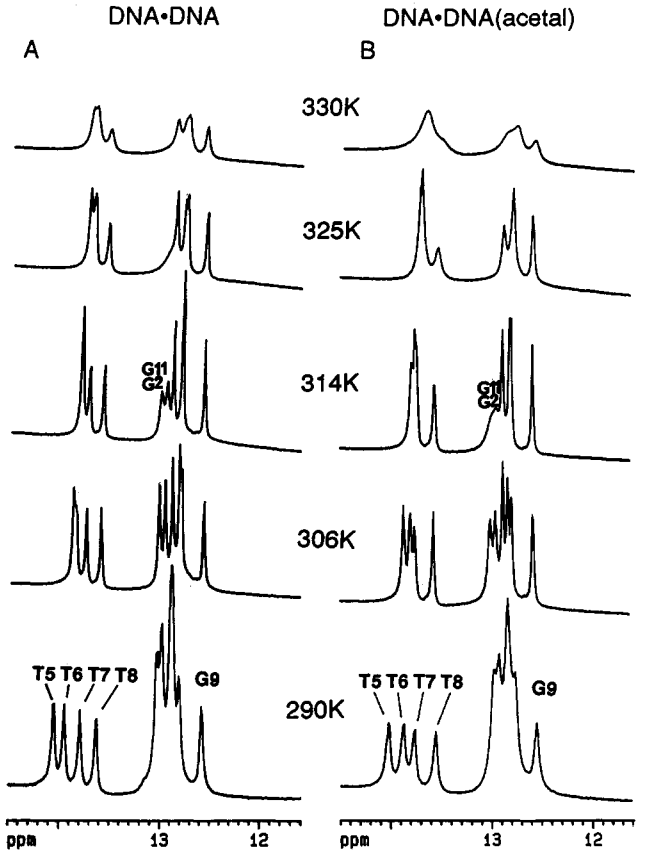

FIGURE 6: Selected one-dimensional imino proton spectra as functions of temperature for (A) duplex II and (B) duplex I. Spectra were recorded in H_2O at every 7 ± 2 °C starting from 5 °C. The time interval between temperature steps was at least 10 min.

Table II: Adenine H2 Proton Related NOE Intensities in DNA·DNA Formacetal Duplex I and Unmodified DNA·DNA Duplex II[a]

NOE correlation	250-ms NOESY		100-ms NOESY	
	duplex II	duplex I	duplex II	duplex I
A108(H2)–T6(H1′)	*8.2*	*8.9*	*3.1*	*3.1*
A108(H2)–A108(H1′)	4.3	5.9	0.8	0.8
A108(H2)–C109(H1′)	7.7	10.8	4.3	5.4
A107(H2)–T7(H1′)	*8.3*	*9.0*	*3.2*	*4.3*
A107(H2)–A107(H1′)	9.4	7.3	1.4	2.0
A106(H2)–A106(H1′)	–	–	–	–
A106(H2)–T8(H1′)	*14.2*	*16.5*	*11.2*	*10.3*
A106(H2)–A107(H1′)	2.1	2.8	1.3	1.1

[a] For experimental details, see Table I. Cross-peak intensities marked by (–) are too weak to be measured. NOE correlations and intensities in italic type are from proton pairs of cross-strand residues.

Table III: $J_{1'2'}$ and $J_{1'2''}$ of Selected Residues of DNA·DNA Formacetal Duplex I and Unmodified DNA·DNA Duplex II[a]

residue	DNA·DNA		(acetal)DNA·DNA	
	$J_{1'2'}$	$J_{1'2''}$	$J_{1'2'}$	$J_{1'2''}$
G4	9.6	6.4	9.2	6.2
T5	8.7	6.0	8.1	6.4
T6	8.2	7.6	9.3	6.8
T7	8.2	~7	8.7	6.1
T8	8.8	7.0	8.6	6.7
G9			~8	~6
C104	8.1	7.0	8.7	6.0
A105	8.9	5.9	9.4	5.8
A106	8.5	5.9	9.4	5.7
A107	8.6	6.7	8.8	6.0
A108	8.3	5.8	8.6	5.6
C109	8.3	6.8	8.0	5.9

[a] Coupling constants were measured from COSY-35 data for both sequences. Error estimation is ±0.5 Hz. The coupling constants of G9 cannot be decided due to the chemical shift degeneracy of 2′ and 2″ protons.

Table IV: Measured Phosphate Oxygen–Proton Distances from B-Form DNA Sequences and NMR-Derived Proton–Proton Distances in Formacetal Duplex II[a]

atom 1	atom 2	distance (O)	atom 1	atom 2	distance (H)
i H1′	*i*+1 O1P	5.2–5.5	T6 H1′	T7 HP1	vw
i H1′	*i*+1 O2P	4.8–5.4	T6 H1′	T7 HP2	vw
i H2′	*i*+1 O1P	5.0–5.3	T6 H2′	T7 HP1	null
i H2′	*i*+1 O2P	3.7–5.0	T6 H2′	T7 HP2	~4.1
i H2″	*i*+1 O1P	4.3–4.8	T6 H2″	T7 HP1	null
i H2″	*i*+1 O2P	2.9–4.2	T6 H2″	T7 HP2	~3.5
i H3′	*i*+1 O1P	2.7–3.8	T6 H3′	T7 HP1	>2.6
i H3′	*i*+1 O2P	2.4–3.2	T6 H3′	T7 HP2	2.6
i+1 H5′	*i*+1 O1P	3.2–3.6	T7 H5′	T7 HP1	3.2 ± 0.2
i+1 H5′	*i*+1 O2P	4.0–4.2	T7 H5′	T7 HP2	vw
i+1 H5″	*i*+1 O1P	2.7–3.4	T7 H5″	T7 HP1	3.4
i+1 H5″	*i*+1 O2P	4.2–4.5	T7 H5″	T7 HP2	vw
i+1 H2′	*i*+1 O1P	4.8–5.1	T7 H2′	T7 HP1	null
i+1 H2′	*i*+1 O2P	3.6–4.2	T7 H2′	T7 HP2	overlap
i+1 H2″	*i*+1 O1P	6.2–6.6	T7 H2″	T7 HP1	null
i+1 H2″	*i*+1 O2P	5.4–5.9	T7 H2″	T7 HP2	null
i+1 H3′	*i*+1 O1P	4.0–4.9	T7 H3′	T7 HP1	overlap
i+1 H3′	*i*+1 O2P	4.6–4.8	T7 H3′	T7 HP2	vw
i H1′	*i*+1 H5′	2.5–4.0	T6 H1′	T7 H5′	3.5
i H1′	*i*+1 H5″	4.3–5.6	T6 H1′	T7 H5″	4.1

[a] O–H distance ranges (in Å) are derived from (1) α-56, β-171, γ-51, δ-140, ε-167, ζ-103 (BI-form; Dickerson et al., 1983), (2) α-41, β-136, γ-38, δ-140, ε-133, ζ-157 (average B-form; Chandrasekaran et al., 1980), and (3) α-72, β-175, γ-57, δ-140, ε-91, ζ-151 (BII-form; Dickerson, 1983). O1P and O2P are phosphate oxygen atoms; HP1 and HP2 are the methylene protons of the formacetal group. *i* and *i*+1 represent two adjacent residues. NMR distances (range ±20%) were obtained from 100-ms mixing time NOESY data unless specified. Some distances were estimated from partially overlapped cross peaks. vw: only observed in the 250-ms mixing time NOESY spectrum.

and the other, an all phosphodiester counterpart (duplex II).

The replacement of a phosphodiester backbone unit by a formacetal linkage has implications for ODN recognition parameters in terms of both imposed electrostatic and steric demands and in terms of the structural homogeneity of the hybrid duplex formed on association with an unmodified oligomer. Thus, backbone modification may affect base pair formation and the relative orientation of the adjacent bases and base pairs. The four thymine and six guanine imino resonances for duplex I are well resolved and exhibit chemical shifts characteristic of Watson–Crick base pairing (Figure 4). The relative NOE cross-peak intensities of T(HN) to the intra-base pair A(H2) and the sequential A(H2) in duplex I are quite comparable to those of duplex II. These results indicate that there is no gross deformation of duplex structure attributable to the incorporation of the formacetal linkage. On the other hand, that small resonance shifts were observed for the thymine imino resonances in duplex I, which are consistently upfield by 0.02–0.05 ppm with respect to duplex II (Figure 5A and Table I), may reflect a slight weakening of the H-bonding between A and T residues and/or a variation in base stacking in duplex I.

Examination of the temperature profile of the imino resonances for duplex I (Figure 6) indicates that the Watson–Crick base pairs for the central 16 residues (eight base pairs) melt simultaneously at about 57 °C, as judged by line broadening, some 4 °C earlier than duplex II. These observations are in good agreement with experimentally determined values of T_m by optical measurements. The fact that base pairs adjacent to the acetal linkage exhibit similar thermal sensitivity to those remote from the modification indicates that the reduced T_m for duplex I is not a consequence of localized premelting at the formacetal modification site. These NMR experiments

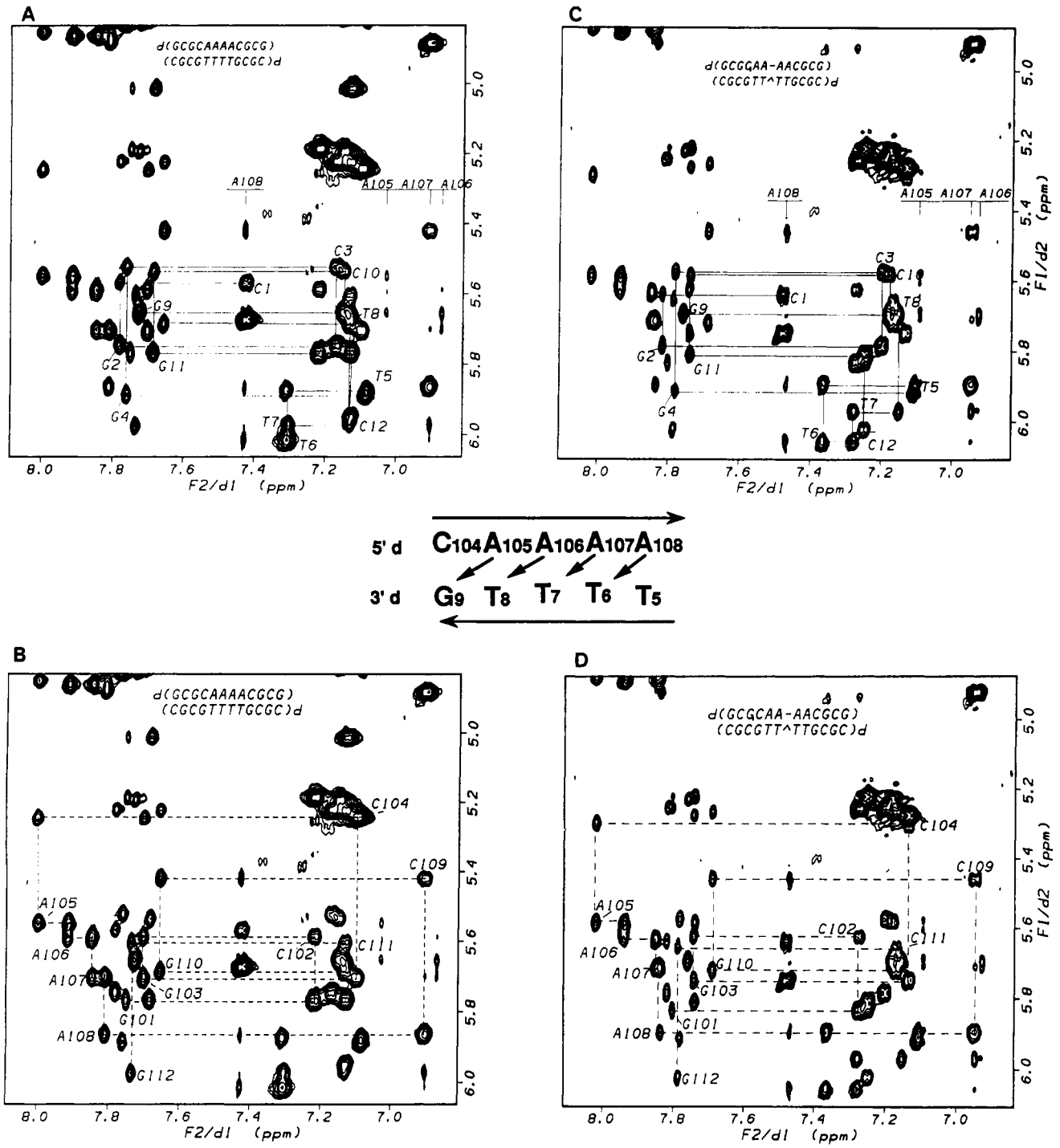

FIGURE 7: Expanded NOESY (250-ms mixing time) spectra recorded in D_2O at 35 °C: (A) d(CGCGTTTTGCGC) strand and adenine H2 NOEs in duplex II [the cross peak at 7.16 and 5.04 ppm is assigned to the NOE from the terminal C12(H6)/(H5)]; (B) d(GCGCAAAACGCG) in duplex II; (C) d(CGCGTT$_{OCH_2O}$TTGCGC) strand and adenine H2 NOEs in duplex I; (D) d(GCGCAAAACGCG) in duplex I. Sequential connectivities linking sugar H1′ (F_1) of the i residue to its own base proton (F_2, cross peaks labeled with residue numbers) and to its 3′-neighboring (i+1) base proton (F_2) in each of the strands in the duplexes are linked with solid lines for both duplex I and duplex II.

were carried out under neutral pH conditions; thus, the effect of base pair lifetime and base catalysis on imino proton line width could not be separated (Guéron et al., 1987). Detailed structural features of duplexes with multiple formacetal substitutions will be examined.

Duplex II exhibits moderate sequential H1′–base proton NOEs (Figure 7) and much weaker H3′–base proton NOEs. These patterns and relative NOE intensities are characteristic of B-type helical conformation (Patel et al., 1987). The coupling constants (Table III) of duplex II for H1′,H2′ are in the range of 8.0–9.5 Hz while for H1′,H2″ are in the range of 5.5-7.0 Hz, and the couplings between H3′ and H2′,H2″ protons are weak. These coupling constants and patterns can be attributed to the C2′-endo-type sugar pucker (Wuthrich, 1986; Chary et al., 1987). Thus, the conformation of duplex II can serve as a reference for assessing the structural perturbation in formacetal-containing duplex I. It is found that the NOSEY spectra (Figure 7) and coupling constants (Figure 8 and Table III) for duplex I are quite comparable to those of duplex II, suggesting that the B-type structural features of the reference sequence, such as helical twist and rise, are maintained on formacetal linkage incorporation.

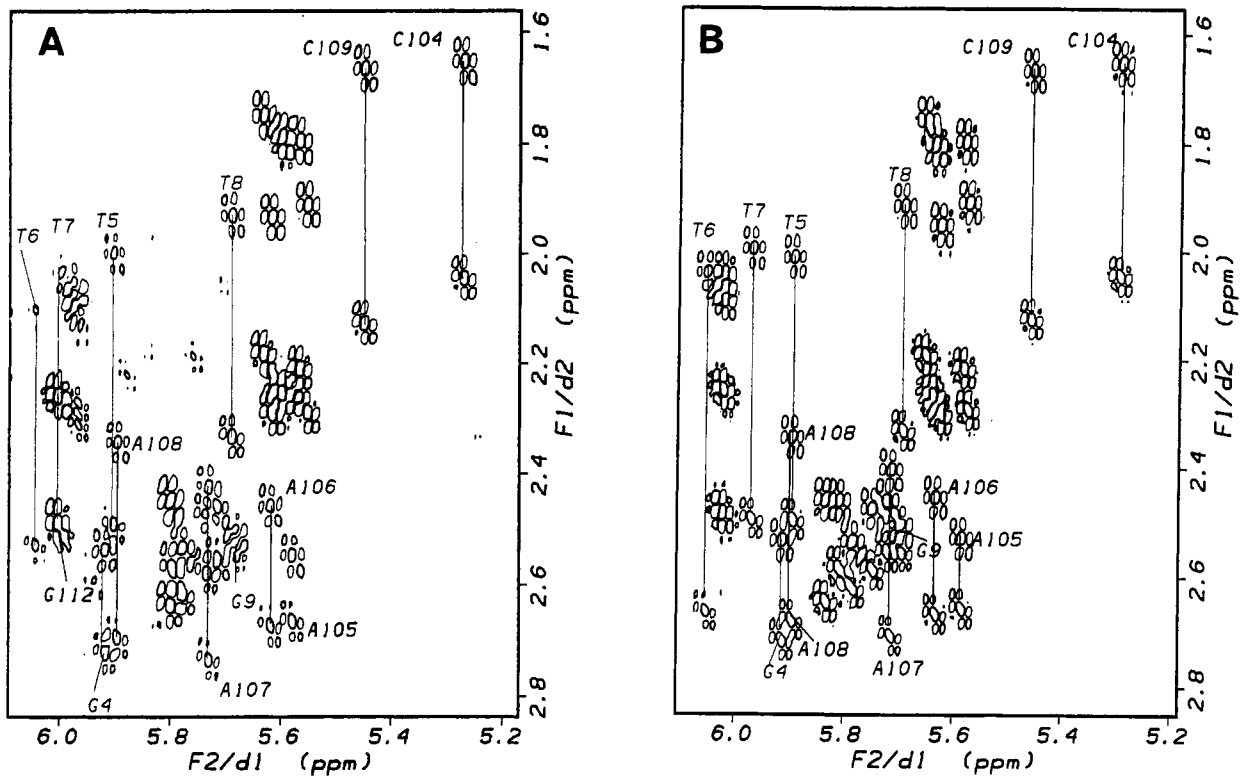

FIGURE 8: Expanded COSY-35 phase-sensitive spectra [H1′ (F_2) and H2′,H2″ (F_1)] recorded in D_2O at 35 °C for (A) duplex II and (B) duplex I. Coupling constants (Table III) were measured from fine antiphase cross-peak splitings displayed in (A) and (B).

Cross-strand NOEs linking the adenine H2 protons to the H1′ proton of an adjacent residue in the complementary strand are indicative for minor groove width. Several cross-strand NOE cross peaks were detected for both duplex I and duplex II (Figure 7A,C) and their intensities, which correlate to distances, compared (Table II). The data set indicates that the minor groove width of duplex I is no wider than that of duplex II, which implies that sugar orientations at the formacetal site as well as all along the backbone are little changed as compared to duplex II.

While the gross structural features of duplex II are maintained in duplex I, there are localized perturbations. These perturbations are evident, for example, in chemical shift differences (Figure 5). Whereas the majority of the proton chemical shifts arising from C and G residues flanking the T_4·A_4 block are identical within experimental error (±0.01 ppm), those associated with the central T and A residues exhibit a quite noticeable shift (Figure 5). Among these shifted resonances, those of T6(H3′) and T7(H5′,H5″) in duplex I are particularly striking (Table I). However, it is likely that these largely reflect variation in chemical rather than structural factors (Figure 1). The most noticeable structural-based shifts were those for the T6(H2′,H2″) resonances for duplex I (Figure 5C,D). Since the chemical shifts of H2′ and H2″ protons are sensitive to the ring current effect from the base moiety through sequential stacking interactions, the observed shifts for T6(H2′,H2″) resonances are most likely due to perturbations in sugar–base stacking at the $T6_{OCH_2O}T7$ step in duplex I relative to its phosphodiester counterpart in duplex II. On the other hand, such structural variation in duplex I must be subtle or else it would cause NOEs in duplex I and duplex II to be largely different.

The backbone geometry of the DNA duplex structure is highly flexible and notoriously difficult to assess, since the particularly relevant proton signals are often extensively overlapped. The formacetal methylene resonances in duplex I, however, are resolved and permit NOE assignment in related spectral regions (Figure 9 and Table IV). The experimentally determined distances linking T7(HP1 and HP2) and the adjacent sugar protons are consistent with the distance ranges for the phosphate oxygen atoms (OP1, OP2) to adjacent sugar protons measured from various B-DNA duplexes (Table IV). The difference in distances associated with T6(H2′,H2″) and T7(H5′,H5″) suggests that the formacetal protons are rotated further away from the H2′,H2″ of the 5′ residue (T6) and that T7(H5′,5″) moves closer to T6(H1′). Quantitative torsional angles about the formacetal site are currently being determined by modeling techniques. The development of a fully refined formacetal ODN structural model is in progress and will be reported in due course.

Conclusion

A comparison of differences in chemical shift, relative intensities of NOE connectivities, and the amplitude of scalar coupling constants leads us to conclude that duplex I assumes a canonical B-type conformation which is similar to that of its phosphodiester counterpart, duplex II. The experimentally derived distances related to the formacetal methylene protons are in agreement with this notion. The NMR data also suggest that structural perturbations attributable to the substitution of a formacetal moiety for a 3′,5′-phosphodiester linkage in duplex DNA are minimal and are localized primarily in the region of the two immediately adjacent residues ($T6_{OCH_2O}T7$). Interestingly, the microscopic melting at this structurally perturbed site echoes the global melting of the duplex. Our study demonstrates that single OCH_2O for PO_2 substitution can be readily accommodated in an ODN duplex with little structural resistance. This conclusion has parallels to the crystallographic study of Heinemann et al. (1991), who demonstrated that CH_2 for O3′ substitution is also viable. These results provide a basis for the study of sequence-specific and cumulative effects of multiformacetal substitution in both

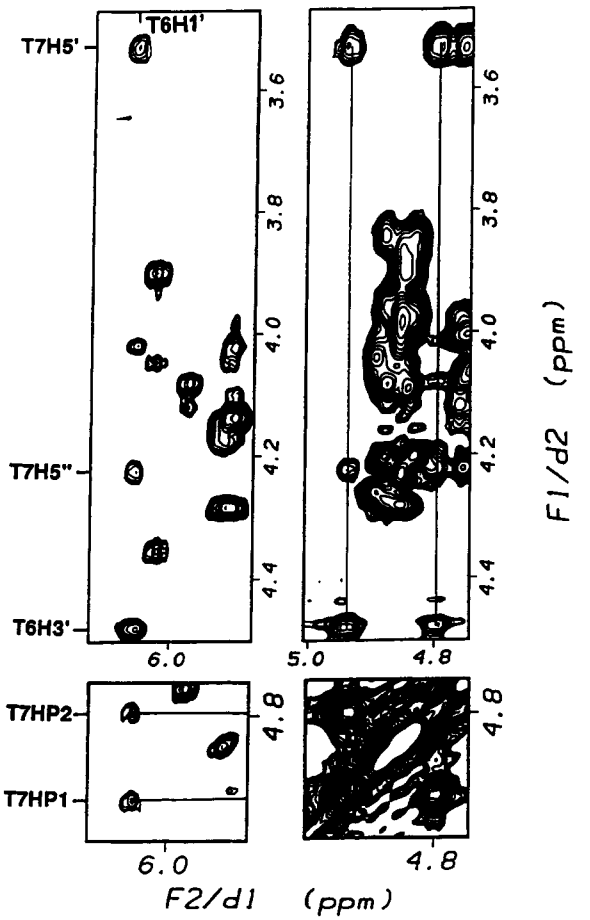

FIGURE 9: Expanded NOESY spectra recorded in D_2O at 35 °C. NOE cross peaks connecting formacetal methylene protons [T7(HP1 and HP2)] with T6(H3) and T7(H5',H5") protons are shown by solid lines, and the corresponding resonance assignments are given along the F_1 axis.

DNA·DNA and DNA·RNA duplexes.

ACKNOWLEDGMENTS

We thank Drs. Stephen Thomson and Robert Anderegg, both of Glaxo Inc. Research Institute, for purification and mass spectral analysis of the oligonucleotides employed in this study.

Registry No. d(GCGCAAAACGCG), 141784-08-9.

REFERENCES

Chandrasekaran, R., Birdasall, D. L., Leslie, A. G. W., & Ratcliff, R. L. (1980) *Nature 283*, 743–745.

Chary, K. V. R., Hosur, R. V., Govil, G., Zu-Kun, T., & Miles, H. T. (1987) *Biochemistry 26*, 1315–1322.

Cruse, W. B. T., Salisbury, S. A., Brown, T., Cosstick, R., Eckstein, F., & Kennard, O. (1986) *J. Mol. Biol. 192*, 891–905.

Dagle, M., Andracki, M. E., Devine, R. J., & Walder, J. A. (1991) *Nucleic Acids Res. 19*, 1805–1810.

Derome, A. (1987) *Modern NMR Techniques for Chemistry Research*, pp 227–230, Pergamon Press, New York.

Dickerson, R. E. (1983) *J. Mol. Biol. 166*, 419–441.

Froehler, B. C. (1986) *Tetrahedron Lett. 27*, 5575–5578.

Froehler, B. C., Ng, P., & Matteucci, M. (1988) *Nucleic Acids Res. 16*, 4831–4839.

Guêron, M., Kochoyan, M., & Leroy, J.-L. (1987) *Nature 328*, 89–92.

Heinemann, U., Rudolph, L.-N., Claudis, A., Morr, M., Heikens, R. F., & Blocker, H. (1991) *Nucleic Acids Res. 19*, 427–433.

Kibler-Herzog, L., Zon, G., Uznanski, B., Whittier, G., & Wilson, W. D. (1991) *Nucleic Acids Res. 19*, 2979–2985.

Lin, S.-B., Blake, K. R., Miller, P. S., & Ts'o, P. O. P. (1989) *Biochemistry 28*, 1054–1061.

Matteucci, M. (1990) *Tetrahedron Lett. 31*, 2385–2388.

McBride, L. J., & Caruthers, M. H. (1983) *Tetrahedron Lett. 24*, 245–248.

Miller, P. S. (1991) *Bio/Technology 9*, 358–362.

Neilson, J., Birll, W. K.-D., & Caruthers, M. H. (1988) *Tetrahedron Lett. 29*, 2911–2915.

Neuhaus, D., & Williamson, M. (1989) *The Nuclear Overhauser Effect in Structural and Conformational Analysis*, pp 104–110, VCH Publishers, Inc., New York.

Patel, D. J., Shapiro, L., & Hare, D. (1987) *Q. Rev. Biophys. 20*, 35–112.

Piotto, M. E., Granger, J. N., Gho, Y., Farchschi, N., & Gorenstein, D. G. (1991) *Tetrahedron 47*, 2449–2561.

Pramanik, P., & Kan, L.-S. (1987) *Biochemistry 26*, 3807–3812.

Schneider, K. C., & Benner, S. A. (1990) *Tetrahedron Lett. 31*, 335–339.

Schneider, K. C., & Benner, S. A. (1991) *J. Org. Chem. 56*, 3869–3882.

Sklenar, V., Miyashiro, H., Zon, G., Miles, H. T., & Bax, A. (1986) *FEBS Lett. 208*, 94–98.

Stephenson, M. L., & Zamecnik, P. C. (1978) *Proc. Natl. Acad. Sci. U.S.A. 75*, 280–284.

Uhlmann, E., & Peyman, A. (1990) *Chem. Rev. 90*, 544–584.

Veeneman, G. H., van der Marel, G. A., van den Elst, H., & van Boom, J. H. (1991) *Tetrahedron 47*, 1547–1562.

Williams, L. D., Egli, M., Ughetto, G., van der Marel, G. A., van Boom, J. H., Quigley, G. J., Wang, A. H.-J., Rich, A., & Frederick, C. A. (1990) *J. Mol. Biol. 215*, 313–320.

Wuthrich, K. (1986) *NMR of Proteins and Nucleic Acids*, John Wiley & Sons, New York.